Analysis of slitless holographic spectrometers implemented by spherical beam volume holograms

Omid Momtahan, Chao Ray Hsieh, Ali Adibi, and David J. Brady

The analysis of a slitless volume holographic spectrometer is presented in detail. The spectrometer is based on a spherical beam volume hologram followed by a Fourier-transforming lens and a CCD. It is shown that the spectrometer is not sensitive to the incident angle of the input beam for the practical range of applications. A holographic spectrometer based on the conventional implementation is also analyzed, and the results are used to compare the performance of the proposed method with the conventional one. The experimental results are consistent with the theoretical study. It is also shown that the slitless volume holographic spectrometer lumps three elements (the entrance slit, the collimator, and the diffractive element) of the conventional spectrometer into one spherical beam volume hologram. Based on the unique features of the slitless volume holographic spectrometer, we believe it is a good candidate for portable spectroscopy for environmental and biological applications.

OCIS codes: 090.7330, 300.6190, 070.2590.

1. Introduction

Diffractive elements such as gratings are the basis of most spectrometers.[1,2] The ambiguity between the incident angle and the wavelength of the input beam, imposed by the basic properties of the grating, is the main limitation on the performance of grating-based spectrometers. The ambiguity is usually removed by using a spatial filter (e.g., the entrance slit) in the input, followed by a collimator, which directly reduces the throughput and increases the total size of the spectrometer. We recently proposed the idea of using a slitless spectrometer to reduce this ambiguity without using the input slit to increase the throughput of the spectrometer and reduce its size.[3] The improvement in throughput is limited by the Lagrange invariant of the optics.[4] Particularly for the incoherent input beam, the throughput of the spectrometer is constrained by the constant radiance theorem.[5] Another feature of using a slitless spectrometer is the capability of obtaining more flexibility in the design and implementation. For example, the need for optical alignment of the slit and the collimator with the rest of the spectrometer elements (which is necessary in conventional spectrometers) is completely avoided by using slitless spectrometers. In this paper we present a practical technique for implementing slitless spectrometers that is based on spherical beam volume holograms (SBVHs). We show that a compact and low-cost spectrometer can be designed by using a SBVH, thus making it a good candidate as a portable device for environmental and biological applications. We recently proposed the idea of using a SBVH as a diffractive element for spectroscopy.[3,6–8] We showed that when the SBVH is read with a collimated beam, a dark crescent forms on the back face of the hologram. The position of the dark crescent is a function of the reading wavelength. Using this method, one can measure the spectral contents of a collimated reading beam based on the location and the intensity of the dark crescents. Besides using the dark crescent, we also showed that the diffracted crescent could be used for spectroscopic applications.[6,7] The diffracted crescents corresponding to different incident wavelengths propagate in different directions and focus in different locations. The main limitation imposed on the performance of a simple SBVH spectrometer based on these two approaches is the ambiguity between the reading incident angle and the wavelength. Any change in the incident angle of the reading beam at a fixed wavelength also changes the location of the dark crescent and the location where the diffracted beam is focused. Therefore neither the

O. Momtahan (omid@ece.gatech.edu), C. R. Hsieh, and A. Abidi are with the School of Electrical and Computer Engineering, Georgia Institute of Technology, Atlanta, Georgia 30332-0250. D. J. Brady is with the Fitzpatrick Center for Photonics and Communication Systems, Duke University, Durham, North Carolina 27708.

Received 10 August 2005; accepted 31 October 2005; posted 11 January 2006 (Doc. ID 64082).

0003-6935/06/132955-10$15.00/0

dark crescent nor the diffracted crescent can be used directly to resolve the spectrum when the hologram is read with a noncollimated or a spatially incoherent beam. Although using a SBVH recorded in reflection geometry can reduce this ambiguity, it cannot eliminate it completely.[8] We recently demonstrated a slitless volume holographic spectrometer based on SBVH that solves the ambiguity problem in the SBVH spectrometers by using a Fourier-transforming lens after the hologram.[3] In this implementation the effect of the incident angle of the reading beam on the locations of the output is minimal. Different wavelength components are separated in different locations at the Fourier plane of the lens even when the input beam is spatially incoherent. As a result, there is no need to use a slit in the input plane of the spectrometer. This is the reason we refer to this spectrometer as a slitless volume holographic spectrometer.

In this paper we focus on the exact analysis of these slitless spectrometers. We also provide an analysis of conventional spectrometers and use the results to compare slitless spectrometers with conventional spectrometers. This analysis is important for understanding the main features and limitations of slitless spectrometers. Furthermore, it is also useful for designing and optimizing these spectrometers both for general spectroscopy and for specific applications. In Section 2 we derive the transfer function of the slitless volume holographic spectrometer. For later comparison, the transfer function of a conventional (slit-based) spectrometer, having a simple plane-wave hologram as a diffractive element, is derived in Section 3. The theoretical evaluations are compared with the experimental results for both cases in Section 4. In Section 5 we compare the performance of the proposed slitless spectrometer with the slit-based holographic spectrometer. Final conclusions are made in Section 6.

2. Transfer Function of the Slitless Volume Holographic Spectrometer

The slitless volume holographic spectrometer is based on a SBVH as a diffractive element. The SBVH is recorded in a holographic medium with thickness L by using a point source and a plane wave as shown in Fig. 1(a). The hologram thickness (L), the incident angle of the plane wave (θ_r), the location of the point source ($-a$, 0, $-d$), and the wavelength of the recording beams (λ) are the design parameters for the recording. The hologram is recorded in the transmission geometry as shown in Fig. 1(a).

The hologram is then used in the spectrometer arrangement shown in Fig. 1(b). The reading beam illuminates the hologram primarily in the direction of the recording spherical beam. Therefore, for the desired range of wavelength, the diffracted beam diffracts mainly in the direction of the recording plane wave as indicated in Fig. 1(b). The Fourier-transforming lens is placed in the main direction of the diffracted beam, and the output is captured in the focal (or Fourier) plane of the lens by using a CCD camera. The focal length of the lens (f) is another

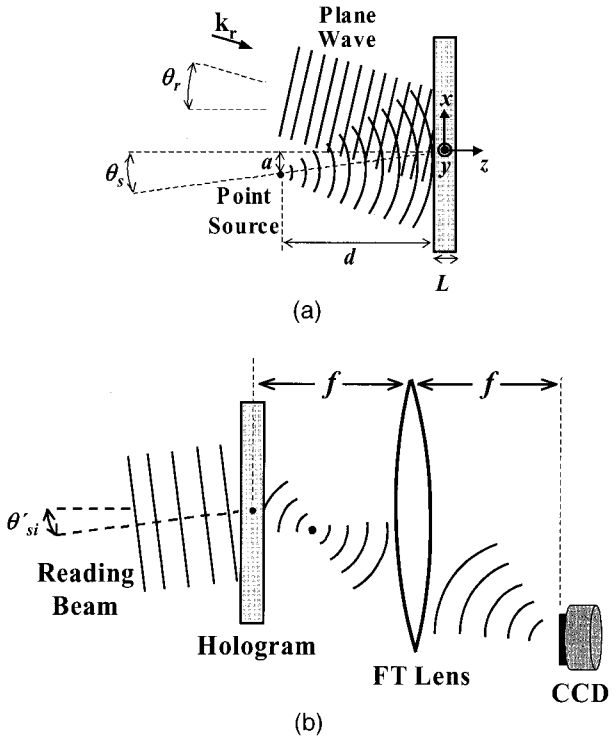

Fig. 1. (a) Recording geometry of a spherical beam volume hologram. The point source is located at ($-a$, 0, $-d$). The reference beam (plane-wave) incident angle is θ_r. A line from the coordinate origin to the point source makes an angle θ_s with the z axis. The thickness of the holographic material is L. (b) Slitless spectrometer configuration. The reading beam is the input to the spectrometer with an incident angle of θ_{si}'. The focal length of the lens is f. The CCD is located at the back focal plane of the lens.

design parameter of the spectrometer. The SBVH in this arrangement can be directly read with a noncollimated beam, and there is no need to use a slit in the input of the spectrometer.[3] Therefore the SBVH is positioned at the very beginning of the system.

To analyze the slitless spectrometer, we first find the optical transfer function of the system shown in Fig. 1(b). The transfer function is defined as the output of the system [at the CCD plane in Fig. 1(b)] to an arbitrary input plane wave (with arbitrary propagation direction) at an arbitrary wavelength λ'.[9] In general, any input beam at wavelength λ' can be represented as a summation of several plane waves at that wavelength. Therefore, using the transfer function, the output of the system to an arbitrary beam can be found at any wavelength. As a result, the output corresponding to any input beam can be found by the analysis of different wavelength components of the beam.

We recently presented the complete analysis of a SBVH when it is read by a collimated beam from the direction of the point source at an arbitrary wavelength.[7] In that analysis the spherical beam was decomposed into several plane-wave components. Each plane wave was assumed to form a hologram with the reference beam. To estimate the diffracted beam, we found the superposition of the diffracted plane waves

from the corresponding holograms when they are read by a collimated beam at wavelength λ'. All the diffraction components were calculated by using the Born approximation. We can use the same approach (as presented in Ref. 7) to study the properties of the slitless volume holographic spectrometer under diffuse light illumination at wavelength λ'. To calculate the output, we first find the transfer function (i.e., the output from a specific input plane wave at wavelength λ') and then incoherently add the output components corresponding to different plane-wave components of the input beam. We assume that the reading beam consists of several plane waves propagating in different directions and with independent random phases with a uniform probability distribution. Throughout the analysis, we also assume that both recording and reading beams have TE polarization [i.e. electric field normal to the incident x–z plane in Fig. 1(a)]. Calculation for the TM polarization (i.e. magnetic field normal to the incident x–z plane) can be found in a similar way.

To find the transfer function, we assume that the electric field of a reading plane wave propagating in the direction $\mathbf{k_i}' = k_{ix}'\hat{\mathbf{a}}_\mathbf{x} + k_{iy}'\hat{\mathbf{a}}_\mathbf{y} + k_{iz}'\hat{\mathbf{a}}_\mathbf{z}$ with amplitude A_i and phase φ_i is represented by

$$E_i(k_{ix}',\ k_{iy}',\ k_{iz}') = A_i \exp[j(k_{ix}'x + k_{iy}'y + k_{iz}'z) + \varphi_i]. \tag{1}$$

From the analysis of Ref. 7, the electric field of the diffracted beam (E_{id}) from a SBVH can be written as

$$E_{id}(x,\ y,\ z) = \frac{\exp[j(k_{rx} + k_{ix}')x]\exp(jk_{iy}'y)}{4\pi^2} \times \int\int \widetilde{E}_{id}(k_x,\ k_y,\ z)\exp[-j(k_x x + k_y y)]\mathrm{d}k_x\mathrm{d}k_y, \tag{2}$$

where k_{rx} represent the x component of the recording plane wave in Fig. 1(a) and the diffracted field in the spatial–spectral domain [i.e., $\widetilde{E}_{id}(k_x, k_y, z)$] is represented by[7]

$$\widetilde{E}_{id}(k_x,\ k_y,\ z) = \frac{j2\pi^2\Delta\epsilon k'^2 L A_i \exp(j\varphi_i)}{\epsilon k_{idz}'}\exp(jk_{idz}'z) \times \mathrm{sinc}\left[\frac{L}{2\pi}(K_{gz} + k_{iz}' - k_{idz}')\right]. \tag{3}$$

In Eq. (3) ϵ is the permittivity of the holographic recording material, $\Delta\epsilon$ is the amplitude of the modulated permittivity, k' is the wavenumber at wavelength λ', and K_{gz} and k_{idz} are given by

$$K_{gz} = k_{rz} - (k^2 - k_x^{\ 2} - k_y^{\ 2})^{1/2}, \tag{4}$$

$$k_{idz}' = [k'^2 - (K_{gx} + k_{ix}')^2 - (K_{gy} + k_{iy}')^2]^{1/2}, \tag{5}$$

where k is the wavenumber at wavelength λ, $K_{gx} = k_{rx} - k_x$, $K_{gy} = -k_y$, and $\mathbf{k_r} = k_{rx}\hat{\mathbf{a}}_\mathbf{x} + k_{rz}\hat{\mathbf{a}}_\mathbf{z}$ is the propagation vector of the recording plane wave.

Now we assume that the Fourier-transforming lens is located at a distance f from the hologram as shown in Fig. 1(b). Although this is not a necessary assumption for the operation of the spectrometer (i.e., the Fourier transform can be obtained by other arrangements of the lens), it simplifies the calculations by eliminating the quadratic phase term that results from the Fourier-transform operation of the lens.[9] In this configuration the CCD is located exactly at the back focal plane (or Fourier plane) of the lens. By assuming the lens is very large compared with the size of the hologram and by using the paraxial approximation, one can write the electric field of the output beam in the Fourier plane of the lens as[9]

$$E_{io}(u,\ v,\ z = 2f) = \frac{A_i}{j\lambda' f} F\{E_{id}(x,\ y,\ L/2)\}\big|_{f_x = u/(\lambda' f)\ \text{and}\ f_y = v/(\lambda' f)}, \tag{6}$$

where u and v are the output coordinates in the focal plane and f_x and f_y are the frequency variables of the two-dimensional Fourier-transform operator $F\{\ \}$ defined as[9]

$$\widetilde{P}(2\pi f_x,\ 2\pi f_y,\ z) = F\{p(x,\ y,\ z)\} = \int\int p(x,\ y,\ z) \times \exp[-j2\pi(f_x x + f_y y)]\mathrm{d}x\mathrm{d}y. \tag{7}$$

From Eq. (2) it is clear that the diffracted beam (E_{id}) can be also represented as a Fourier transform. Therefore Eq. (6) can be rewritten as

$$\begin{aligned} E_{io}(u,\ v,\ 2f) &= \frac{A_i}{j\lambda' f} F\left\{\exp[j(k_{rx} + k_{ix}')x]\exp(jk_{iy}'y)F^{-1}\{\widetilde{E}_{di}(k_x,\ k_y,\ 2f)\}^{x\to -x}_{y\to -y}\right\}_{f_x = u/(\lambda' f)\ \text{and}\ f_y = v/(\lambda' f)} \\ &= \frac{A_i}{j\lambda' f}\widetilde{E}_{id}[-(2\pi f_x - k_{rx} - k_{ix}'),\ -(2\pi f_y - k_{iy}'),\ 2f]\big|_{f_x = u/(\lambda' f)\ \text{and}\ f_y = v/(\lambda' f)} \\ &= \frac{A_i}{j\lambda' f}\widetilde{E}_{id}(-k'u/f + k_{rx} + k_{ix}',\ -k'v/f + k_{iy}',\ 2f). \end{aligned} \tag{8}$$

Substituting $\widetilde{E}_{id}(k_x, k_y, z)$ from Eq. (3) and replacing k_x and k_y by their corresponding arguments according to Eq. (8), the transfer function (the output electric field) can be written as

$$\begin{aligned} H(u, v, z = 2f, \lambda') &= E_{io}(u, v, 2f)/[A_i \exp(j\varphi_i)] \\ &= \frac{j2\pi^2 \Delta\epsilon k'^2 L}{\epsilon_0 \left[k'^2 - (k'u/f)^2 - (k'v/f)^2\right]^{1/2}} \\ &\quad \times \exp\{j2f\left[k'^2 - (k'u/f)^2 - (k'v/f)^2\right]^{1/2}\} \\ &\quad \times \operatorname{sinc}(L/2\pi\{k_{rz} - \left[k^2 - (k'u/f - k_{rx} - k_{ix}')^2 - (k'v/f - k_{iy}')^2\right]^{1/2} \\ &\quad + k_{iz}' - \left[k'^2 - (k'u/f)^2 - (k'v/f)^2\right]^{1/2}\}). \end{aligned} \tag{9}$$

As seen from Eq. (9), the amplitude of the transfer function (the electric field in the output, E_{io}) is a function of the output coordinate (u, v). Note that the maximum of H occurs at the output coordinates for which the argument of the sinc function in Eq. (9) is zero. The locus of the maximum electric field is also a function of the reading-beam direction represented by k_{ix}' and k_{iy}' in Eq. (9). However, the effect of the direction of the reading beam on the location of the diffracted beam in the output is minimal for the practical range of angles as we will examine below.

To find the output to an incoherent beam, we should add the output intensities of all of the input plane-wave components [each one is a plane wave in Eq. (1) with a random phase]. Therefore the total output intensity is

$$\begin{aligned} I_o(u, v, 2f) &= \int A_i{}^2(k_{ix}', k_{iy}') \, |H(u, v, z \\ &= 2f, \lambda')|^2 \mathrm{d}k_x' \mathrm{d}k_y' \\ &= \int |E_{io}(u, v, 2f)|^2 \mathrm{d}k_x' \mathrm{d}k_y', \end{aligned} \tag{10}$$

where the integration is over all the spatial-frequency components (k_{ix}' and k_{iy}') of the input reading beam. It should be noted that all the parameters should be calculated considering the refractive index of the holographic material.

Figure 2 shows the intensity distribution in the output for the region corresponding to the CCD area (6.9 mm × 4.6 mm) when a typical hologram is read with a spatially incoherent beam. In this calculation the reading beam is modeled as a series of plane-wave components with equal amplitudes and independent random phases for the incident angles in the range from $-\theta_s'$ to θ_s' with $2\theta_s'$ the actual divergence angle of the input beam in the actual experiments in both

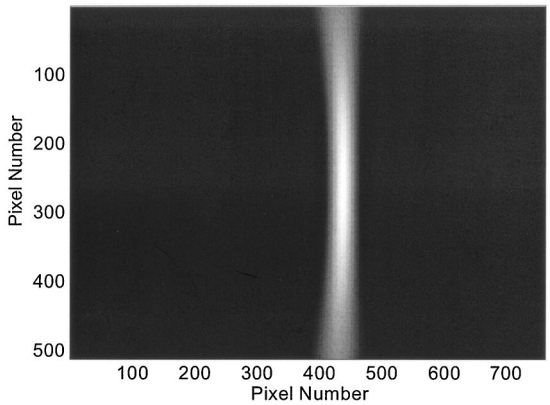

Fig. 2. Theoretical intensity distribution in the output of the slitless holographic spectrometer estimated for the region corresponding to the CCD area when the hologram is read with a spatially incoherent reading beam. The incident angle of the reading beam is assumed to be from −5° to 5° measured in the air in both the x and the y directions corresponding to the total solid angle of 0.03 sr. The hologram is assumed to be recorded by using the setup in Fig. 1(a) with $d = 4$ cm, $L = 300$ μm, $\theta_r = 46°$, and $\theta_s = -9°$. The reading wavelength is 532 nm, which is equal to the recording wavelength. The refractive index of the recording material is assumed to be 1.5.

x and y directions. The hologram is assumed to be recorded by using the setup in Fig. 1(a) with $d = 4$ cm, $L = 300$ μm, $\theta_r = 46°$, and $\theta_s = -9°$. The reading wavelength is $\lambda' = 532$ nm and is equal to the recording wavelength (λ). The refractive index of the recording material is assumed to be 1.5. The results in Fig. 2 are calculated by using $\theta_s' = 5°$. As is seen from Fig. 2, the output is a single crescent, which is very similar to the output when a single collimated beam reads the hologram. Therefore the outputs of different plane-wave components (or directions) of the reading beam at a single wavelength almost overlap at the same location in the output plane.

Note that for the experimental measurements, the Fourier-transforming lens is mounted perpendicular to the direction of the diffracted beam as shown in Fig. 3. Compared with the arrangement shown in Fig. 1(b), the experimental configuration is rotated and also shifted in the space domain. The rotation of the

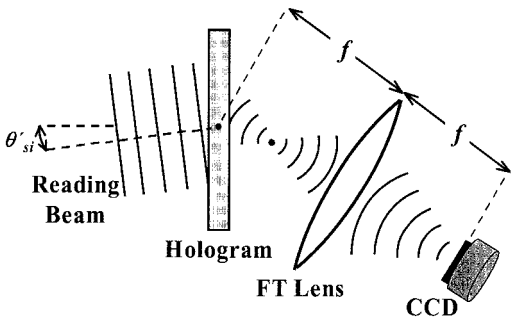

Fig. 3. Experimental arrangement of the slitless spectrometer. All the parameters are the same as those given in the caption of Fig. 1 (b).

lens is equivalent to the rotation (or a phase shift) of the incident beam in paraxial approximation. Therefore the effect is equivalent to a shift in the Fourier domain or a shift in the position of the diffracted crescent in the Fourier plane of the lens. Also, the shifts in the lens coordinate, as it is seen in Fig. 3 compared with Fig. 1(b), results in a shift in the Fourier coordinates. Therefore the difference in the theoretical configuration with the experimental setup is a shift in the Fourier plane and can be compensated for with a constant shift. The theoretical configuration reduces complicated conversions between rotated coordinates and is easier to analyze. On the other hand, the main benefit of mounting the lens in the direction of the diffracted beam in the experimental setup is to reduce the vignetting effect caused by the limited size of the lens. Also, the aberration introduced by the lens is minimal in this configuration.[9]

3. Transfer Function of a Spectrometer Based on a Plane-Wave Hologram

To better understand the properties of the slitless volume holographic spectrometer, we compare it with a spectrometer based on a conventional implementation shown in Fig. 4. This spectrometer consists of a 4*f*-like system that images the input to the output at each wavelength. The hologram crosses the Fourier plane of the first lens and contains its focal point as shown in Fig. 4. The angle between the hologram and the input plane (α) in the spectrometer setup is determined by the desired wavelength range of operation and the hologram recording parameters (i.e., the direction and the period of the grating). The hologram is recorded with two interfering plane waves at wavelength λ by using transmission geometry. The total

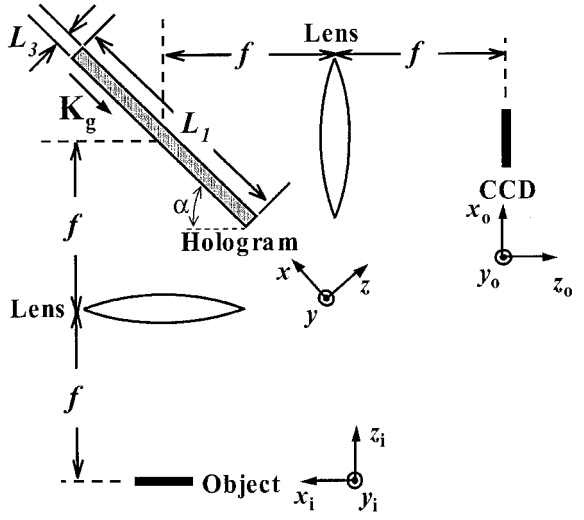

Fig. 4. Basic arrangement of a spectrometer that uses a plane-wave hologram as the diffractive element. The hologram dimensions are shown in the figure. The hologram height (the dimension in the y direction) is assumed to be L_2 (not shown in the figure). The focal length of both lenses is f. The input object is usually a slit in the y_i direction.

angle between the recording beams in the air is 2θ, and the beams have equal incident angles (measured between each beam and the normal to the hologram surface). Therefore the grating vector ($\mathbf{K_g}$) is parallel to the hologram's larger surface (parallel to the x axis in Fig. 4), and its magnitude is $4\pi \sin(\theta)/\lambda$. Using the Born approximation,[10] we can write the output corresponding to a monochromatic input point source at wavelength λ' located at (x_i, y_i) (i.e., the point-spread function) as

$$h(x_i, y_i; x_o, y_o; \lambda') = C\,\mathrm{sinc}\left(\frac{L_1}{2\pi}k_1\right) \times \mathrm{sinc}\left(\frac{L_2}{2\pi}k_2\right)\mathrm{sinc}\left(\frac{L_3}{2\pi}k_3\right), \tag{11}$$

$$k_1 = \frac{2\pi}{\lambda'}\left[\left(\frac{-x_i}{f}+1\right)\cos(\alpha) - \left(\frac{x_o}{f}-1\right)\sin(\alpha)\right] + K_g, \tag{12}$$

$$k_2 = \frac{2\pi}{\lambda'}\left(\frac{y_i}{f}+\frac{y_o}{f}\right), \tag{13}$$

$$k_3 = n\,\frac{2\pi}{\lambda'}\left[-\left(\frac{-x_i}{f}+1\right)\sin(\alpha) - \left(\frac{x_o}{f}-1\right)\cos(\alpha)\right], \tag{14}$$

where (x_o, y_o) represent the output coordinates; f is the focal length of the lenses; n is the index of refraction of the holographic material; K_g is the magnitude of the grating vector; and L_1, L_2, and L_3 are the hologram dimensions in the x, y, and z directions, respectively. The amplitude factor C is a function of the diffraction efficiency of the hologram and can be estimated from the Born approximation when the amplitude modulation of the permittivity (or the modulated refractive index) of the hologram is given. Since the throughput of the spectrometer is an important design factor, the hologram should have a high diffraction efficiency. The ideal case would be a hologram with 100% diffraction efficiency. Therefore the Born approximation is not accurate for estimating such diffraction efficiencies, and more accurate models, such as the Kogelnik method[11] or the rigorous coupled-wave analysis (RCWA) method,[12] must be used. The RCWA method considers all the reflected and transmitted orders for diffraction and yields to accurate numerical estimation in most cases.[12] In the Kogelnik method, which provides the closed-form solution, only the zeroth and first-order diffraction for the transmitted beam is considered and might not result in a very accurate estimation when reflection at the boundaries is significant. It should be noted that the results from the Kogelnik and RCWA approaches are exactly the same if we

consider that there is no reflection from the faces of the hologram due to a change in the refractive index from air to material and that the hologram is a Bragg grating (only zeroth and first-order diffraction).

In both of the accurate approaches (RCWA and Kogelnik) the hologram is assumed to have infinite transverse dimensions. While the Born approximation is a valid assumption for weak holograms, as is illustrated in Eq. (11), it provides a closed-form solution and can also be used for a hologram with finite lateral dimensions. When the hologram becomes strong, the depletion of the reading beam should be taken into account for the Born approximation. Comparing the Born approximation with the Kogelnik method, we expect that the depletion of the reading beam results in the variation of the diffraction efficiency as a $\sin^2$ of the constant C in Eq. (11). It means that we can simply use the "sin" of the point-spread function in Eq. (11), and the results would be similar to those we can obtain from the Kogelnik method for all practical purposes. We refer to this method as the modified Born approximation, and we calculate the diffraction efficiency (η_{MB}) as $\eta_{MB} = \sin^2(\sqrt{\eta_{\mathrm{Born}}})$, where η_{Born} is the diffraction efficiency calculated by using the Born approximation.

Figure 5(a) shows the diffraction efficiency of a typical strong hologram as a function of normalized modulated permittivity ($\Delta\epsilon/\epsilon$) when it is calculated by using the Born approximation, the modified Born approximation, and the Kogelnik method. The hologram is assumed to be recorded by using two plane waves at a 532 nm wavelength. Each plane wave has an incident angle of 35° in air. The refractive index of the recording material is $n = 1.5$. The hologram is read with one of the beams to match the Bragg condition. The hologram thickness is assumed to be 100 μm. The polarization of the recording beams is TE. As is seen in Fig. 5(a), the maximum diffraction efficiencies calculated by using the modified Born approximation and the Kogelnik method are exactly the same. Note that using the Born approximation for large permittivity modulations results in diffraction efficiencies greater than 100% that are meaningless. From Fig. 5(a) it is clear that the Born approximation is valid for diffraction efficiencies less than 10%. We have found similar behavior for TM polarization (i.e., magnetic field perpendicular to the plane of incidence). Figure 5(b) shows the diffraction efficiency for the same hologram and for the maximum permittivity modulation $\Delta\epsilon = 0.0062\epsilon$ when the incident angle of the reading beam is changed from 32° to 38° outside the material. The reading beam at a 532 nm wavelength has TE polarization. There is an excellent agreement between the modified Born approximation and the Kogelnik method. Again, similar results were obtained for TM polarization. Therefore the modified Born approximation can be used with good accuracy for the analysis of the strong grating, while it provides an analytic solution for holograms with finite lateral dimensions. Note that we have not yet developed a mathematical proof for the equivalence of the two techniques (modified Born and Kogelnik), but all our observations suggest a very good agreement between them.

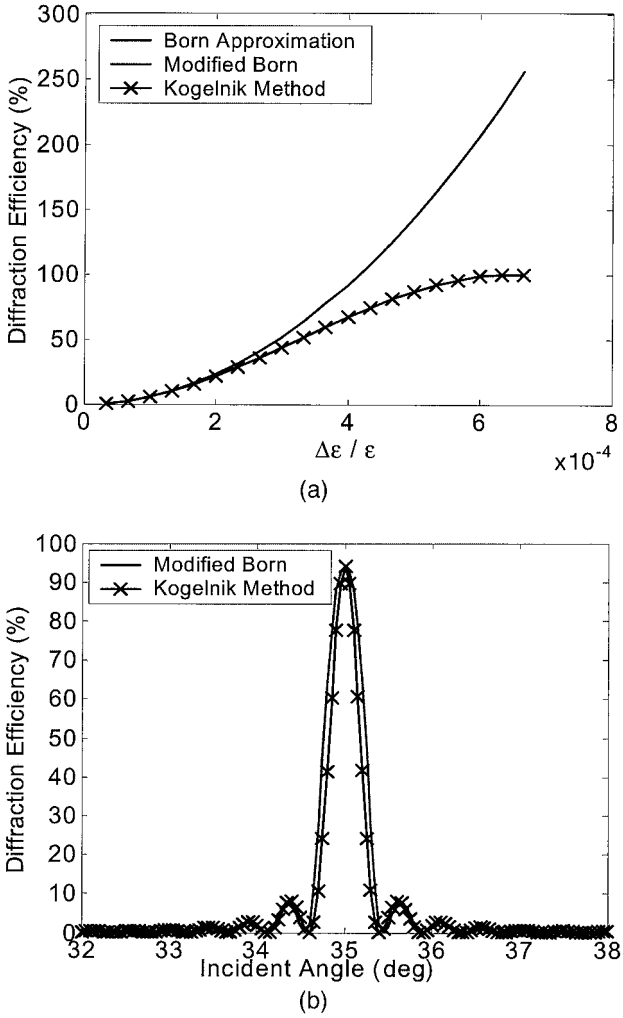

Fig. 5. Diffraction efficiency of a plane-wave hologram (a) as a function of normalized modulated permittivity ($\Delta\epsilon/\epsilon$) for a Bragg-matched reading beam and (b) as a function of the incident angle of the reading beam for $\Delta\epsilon/\epsilon = 0.0062$, calculated by using the Born approximation and the Kogelnik method. The hologram is assumed to be recorded by using two plane waves at a 532 nm wavelength. Each recording plane wave has an incident angle of 35° in air. The refractive index of the recording material is $n = 1.5$. The hologram thickness is assumed to be 100 μm. The polarization of the recording beams is TE. The diffraction efficiency in the modified Born approximation (η_{MB}) is calculated as $\eta_{MB} = \sin^2(\sqrt{\eta_{\mathrm{Born}}})$, where η_{Born} is the diffraction efficiency calculated by using the Born approximation as described in the text.

For finding the complete output of the spectrometer, we assume that the input is a spatially incoherent source with uniform intensity I_i over a slit in the input plane. We also assume that the slit sizes in the x and y directions are s_x and s_y, respectively. Therefore the output corresponding to this input can be found from the convolution of $|h|^2$ [from Eq. (11)] with the intensity distribution of $I_i\,\mathrm{rect}(x/s_x)\,\mathrm{rect}(y/s_y)$, where the rectangle function [$\mathrm{rect}(u)$] is defined as

$$\mathrm{rect}(u) = \begin{cases} 1 & |u| < 1/2 \\ 0 & \text{otherwise} \end{cases}. \tag{15}$$

When the diffraction efficiency of the hologram is high, we can use the modified Born approximation by the convolution of $\sin(|h|)^2$ with the intensity distribution of the input slit.

4. Experiments

In this section the theoretical results are compared with the experimental results for both the slitless volume holographic spectrometer and the conventional holographic spectrometer. For all the experiments, the holograms were recorded in an Aprilis photopolymer[13] with a refractive index of 1.5. The recording wavelength was 532 nm. The polarization of the recording beams was TE, and the holograms were recorded in transmission geometry.

For the SBVH, the hologram was recorded by using the setup in Fig. 1(a) with $d = 4$ cm, $\theta_r = 46°$ (in air), $\theta_s = -9°$ (in air), and $L = 300$ μm. For the conventional spectroscopy, we used a plane-wave hologram recorded by using two coherent plane waves at $\lambda = 532$ nm, each having an incident angle of $\theta = 35°$ in air with respect to the normal to the surface of the recording material. The hologram dimensions were 1 cm, 1 cm, and 100 μm, corresponding to L_1, L_2, and L_3 in Fig. 4, respectively. The reason that a thinner hologram was used for this case was to obtain broader wavelength selectivity.

The reading configuration for the SBVH is shown in Fig. 3. A beam from a monochromator with an output aperture size of 1 mm reads the SBVH after it passes through a rotating diffuser. The full width at half-maximum (FWHM) of the output of the monochromator was ~7.5 nm for the range of wavelength used in the experiment. The rotating diffuser is placed adjacent to the hologram (not shown in Fig. 3) to generate a spatially incoherent reading beam that reads the hologram from almost every direction. The focal length (f) of the Fourier-transform lens was 10 cm. The diffracted beam was monitored by using a cooled CCD camera with 9 μm × 9 μm pixels mounted at the focal plane of the lens. The experimental result for the reading beam with three wavelength components at 492, 532, and 562 nm (from left to right, respectively) is shown in Fig. 6(a). The output corresponding to each wavelength was obtained separately, and the results were added to obtain this figure. The theoretical results corresponding to the experimental ones are shown in Fig. 6(b). The theoretical results were obtained from the analysis presented in Section 2 for the experimental parameters. Figure 6 shows good agreement between the theoretical and the experimental results. Note that the sidelobes in the experimental results [Fig. 6(b)] look stronger than those in the theoretical results [Fig. 6(a)]. We believe this is because of the high diffraction efficiency of the SBVH in the experimental case that is not precisely modeled using the Born approximation.

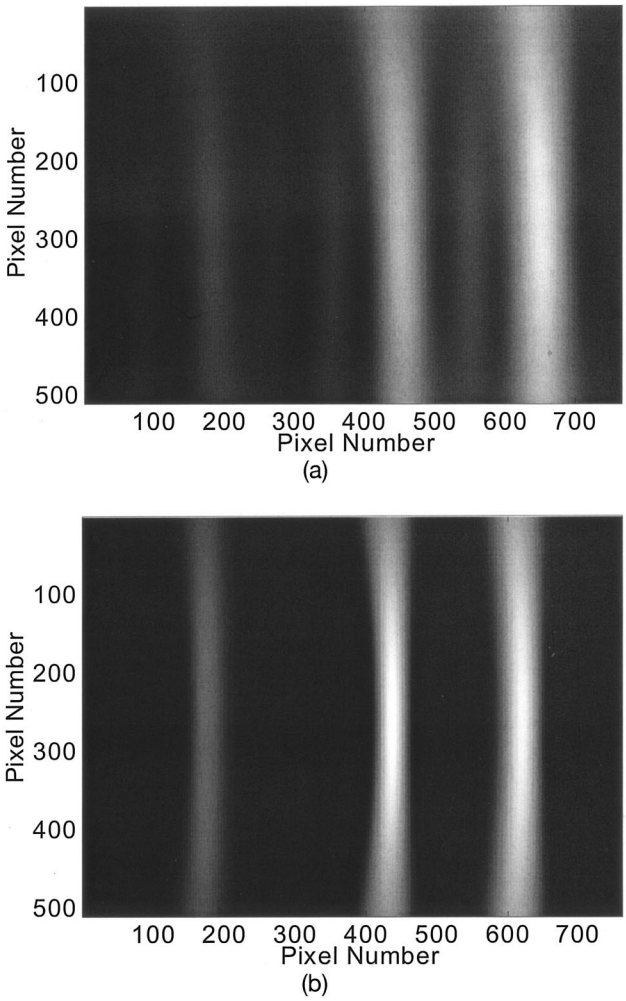

Fig. 6. Output of the slitless spectrometer for an input beam with wavelength components at 492, 532, and 562 nm obtained from (a) experiment and (b) theory. The SBVH was recorded by using the parameters in Fig. 1 (a) with $d = 4$ cm, $\theta_r = 46°$ (in air), $\theta_s = -9°$ (in air), $L = 300$ μm, and $f = 10$ cm. The recording wavelength was 532 nm. The pixel size of the CCD camera was 9 μm × 9 μm. Note that the sidelobes in the experimental results look stronger than those in the theoretical results. We believe this is because of the high diffraction efficiency of the SBVH in the experimental case that is not precisely modeled using the Born approximation.

For the conventional plane-wave holographic spectrometer (with slit present), the hologram was read by a beam obtained by passing white light through the monochromator described earlier, with a FWHM of 7.5 nm centered at a 532 nm wavelength. The beam was collimated and passed through a square opening (or slit) with dimensions of 140 μm × 140 μm. The focal length of the lenses was 6.5 cm. The output was monitored by using a commercial CCD camera with a pixel size of 9.8 μm × 9.8 μm. Note that the CCD in this case is different from that used in the previous experiment; however, this does not affect our results. The intensity distribution along the x axis in the output plane (x_o axis in Fig. 4) is shown in Fig. 7(a). The intensity distribution was also found theoretically by taking into account the

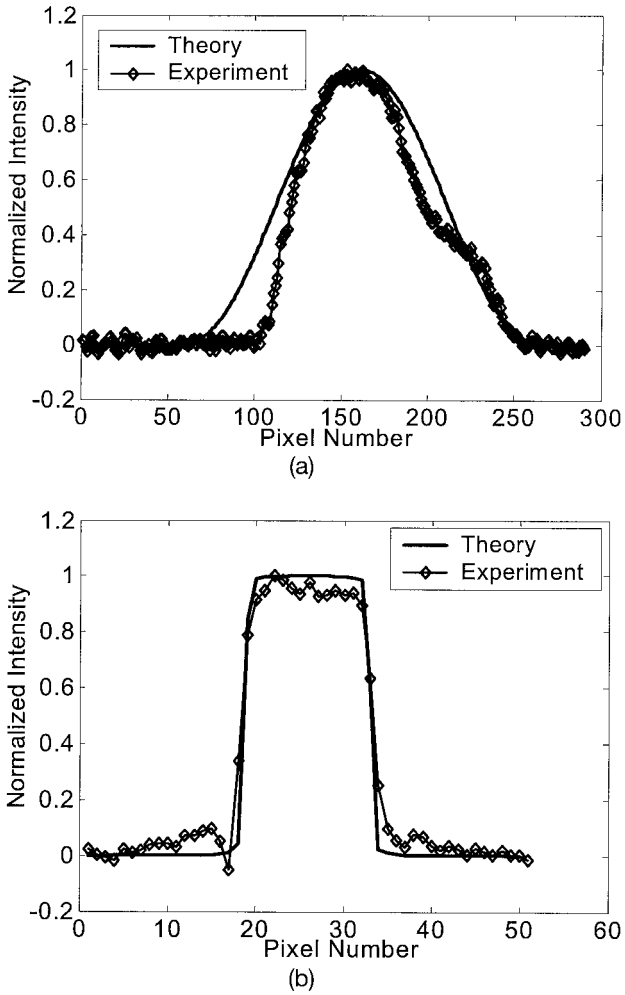

Fig. 7. Distribution of the output intensity of the conventional spectrometer shown in Fig. 4 obtained from both theory and experiment for (a) x_o direction and (b) y_o direction. The hologram dimensions were $L_1 = 1$ cm, $L_2 = 1$ cm, and $L_3 = 100$ μm. The focal length of both lenses was 6.5 cm. The hologram was recorded at 532 nm by using two plane waves, each with an incident angle of 35° measured in air. The hologram was read by a beam at 532 nm obtained by passing white light through a monochromator. The FWHM of the output spectrum of the monochromator at a 532 nm wavelength was 7.5 nm. The beam was collimated and passed through a square opening with dimensions of 140 μm × 140 μm (the object in Fig. 4). The square shape was selected to show the difference in the output for different input directions. The output was monitored by using a commercial CCD camera with a pixel size of 9.8 μm × 9.8 μm. Note that only the range of CCD pixels corresponding to a significant output signal is shown.

FWHM of the reading beam and is shown in Fig. 7(a). The same results for the y axis in the output plane (y_o axis in Fig. 4) are shown in Fig. 7(b). The main reason for the difference in the output along the x and y directions is the finite linewidth of the monochromator. Since the grating vector is perpendicular to the y axis (Fig. 4), the broadening is observed only in the x direction. This effect is observed in both theoretical and experimental results. In the y direction the output is almost identical to the input in both the theory and the experiment. As is seen from these figures, there is a good agreement between theoretical and experimental results for the conventional spectrometer.

5. Comparison

In this section we use the theoretical model we derived so far to qualitatively compare the performance of spectrometers implemented based on two methods. We start by finding the output of the conventional spectrometer to a monochromatic and incoherent input beam. We then find the response of the slitless spectrometer to the same input and show the similarities between the two systems. We then discuss the effect of the different components on the performance of each system.

We assume that the input to the conventional spectrometer, shown in Fig. 4, is an incoherent beam at wavelength λ', consisting of several plane-wave components with random relative phases. A slit of the width s_w is placed in the object plane in Fig. 4 to allow a small portion of each plane-wave component to enter the spectrometer. For each monochromatic plane wave, the conventional spectrometer is equal to a $4f$ imaging system with the point-spread function given by Eq. (11). Therefore the output is a slit with the width s_w that is blurred with the point-spread function h. The effect of the change in the direction of the input plane wave does not change the location of the output since the $4f$ system images the input slit into the same output image at each wavelength. Therefore the total output for the incoherent input is equal to the incoherent (or intensity) summation of the outputs of all plane-wave components. Note that the performance of the $4f$ system is precise into the paraxial regime and is limited to a vignetting effect of the first Fourier-transforming lens (the lens before the hologram).[9]

We derived the output of the slitless spectrometer to an incoherent input in Section 2. We showed that the output was a portion of a ring (or a crescent) as shown in Fig. 2. We assumed that the monochromatic incoherent input beam is a summation of several plane-wave components with random phases. The output of each plane wave is a crescent in the output. The crescents for different plane-wave components overlap in the output at a location that is a function of the input wavelength. Therefore the total output is the incoherent (or intensity) summation of the individual crescents at the output plane.

Comparing the operating principles of the two spectrometers yields several similarities. The output corresponding to a monochromatic input plane wave does not change with the incident angle of the plane wave. Therefore the output to a monochromatic incoherent beam can be found by adding the output intensities of individual plane-wave components. Also, we found that the spatial-intensity pattern of the spectrometer output is a function of the input wavelength in both cases. In the conventional spectrometer the output is a narrow slit, while in the slitless spectrometer it is a narrow crescent for each monochromatic input beam. Since the output of the con-

ventional spectrometer is almost the image of the input slit, we can substitute the rectangular input slit with a crescent-shaped slit (a transparency function similar to the beam shape in Fig. 2), and the results of the conventional spectrometer would be the same as those of the slitless spectrometer. This suggests that the two systems operate similarly. By comparing the configuration of the slitless spectrometer (Fig. 3) with the conventional spectrometer (Fig. 4), we conclude that the role of the SBVH is to implement three elements of the conventional spectrometer [i.e., the input slit, the input lens, and the diffractive element (plane-wave hologram)] into one element (i.e., the SBVH). To be more specific, in the slitless spectrometer the input lens is implemented with a grating formed by a spherical beam and a plane wave. Also, the role of the slit in the conventional spectrometer is implemented by the Bragg selectivity of the volume hologram.

To further compare the two systems we must take into account some practical limitations such as the numerical aperture (NA) of the lenses. For example, the NA of the lens used to form the point source for recording the SBVH is the key parameter that specifies the range of the incident angle of the input beam of the spectrometer (reading beam), which by itself defines the throughput. Similarly, the NA of the first lens in the arrangement of the conventional implementation is the important parameter in finding the range of the incident angle of the input beam to the system. For example, if the input source is a fully incoherent source that emits light in all directions, only a portion of the energy that is distributed over a 4π sr solid angle goes into the system. Therefore a limitation exists on the acceptance input power owing to the limited NA of the practical lenses in both cases. Lenses with high NA are difficult and costly to make. For the conventional spectrometer, the lens is a part of the actual system. However, in the slitless spectrometer, the lens is used to record the hologram that is installed in the system. Therefore the cost per device of the slitless spectrometer with a lens with high NA is much less than that of the conventional spectrometer with a similar input-lens performance.

For the dispersive element that should be used in each system, both the diffraction efficiency and the wavelength selectivity of the holograms are important. In the conventional spectrometer the grating should be thin (thickness in the range of a few micrometers) to diffract a large range of the wavelength with a high diffraction efficiency. On the other hand, the diffraction efficiency of the hologram reduces with decreasing material thickness.[10–12] The main challenge in fabricating the holograms for conventional spectrometers is maximizing the diffraction efficiency for thin material. In the slitless spectrometer, in contrast to the conventional spectrometer, the range of the diffracted wavelength is limited by the divergence angle of the recording point source. The wider the angle is, the larger the wavelength range of the operation is. Therefore there is no direct relation (or trade-off) between the operating range of the wavelength and the thickness of the material. However, the hologram thickness defines the crescent thickness and therefore the wavelength resolution. The thicker the hologram, the narrower the crescent, and the higher the resolution. The role of the thickness of the hologram in the slitless spectrometer is similar to the width of the slit in the conventional spectrometer. As we mentioned before, increasing the material thickness results in a higher dynamic range for holographic recording. In the slitless spectrometer increasing the material thickness improves the peak diffraction efficiency of the crescent. Therefore the peak diffraction efficiency and the wavelength resolution can be improved simultaneously by using a thicker hologram. This makes the fabrication of the SBVH very easy for the slitless spectrometer. Furthermore, we can multiplex more SBVHs to obtain multiple (thin) crescents for each wavelength to avoid losing the throughput of the spectrometer. The detection parts of both devices are almost the same, and we do not consider the effects of the CCD in our analysis.

Implementing three different elements of the conventional spectrometer into one element in the proposed slitless spectrometer makes the device more compact. Also, the Fourier-transform lens can be placed quite close to the hologram to further reduce the total size of the device. Since the slitless spectrometer uses fewer optical elements, it is less sensitive to alignment. Also, removing the input slit and lens reduces the total cost of the device. The SBVH is placed at the very beginning of the device, and the coupling to the device is very easy. All these features make the proposed slitless spectrometer a very good candidate for low-cost, portable spectrometers. Furthermore, replacing the input slit and lens with a volume hologram provides us with more design flexibility, especially for application-specific spectrometers, through optimization of the volume hologram that we record. Some possibilities include multiplexing several SBVHs to develop a more complex spatial–spectral pattern in the spectrometer output (compared with a simple crescent) to implement multimode–multiplex spectroscopy. Such complex (and, in the ideal case, optimal) volume holograms in the slitless architecture would implement complex slits in conventional architecture that are more expensive and more alignment sensitive. Note that by using a more complex volume hologram, it is even possible to remove the Fourier-transform lens and to develop an ultracompact spectrometer, which is composed of only a volume hologram and a CCD camera (or a detector array).

6. Conclusion

We presented here a complete analysis of the slitless spectrometer based on a spherical beam volume hologram (SBVH). The proposed spectrometer consists of a SBVH, followed by a Fourier-transform lens and a CCD. We derived the transfer function of the slitless spectrometer and showed that the output was not sensitive to the incident angle of the input beam. We showed that the theoretical results agree well

with the experimental data. Also, we found the transfer function of the conventional spectrometer that consists of an entrance slit, a collimating lens, a plane-wave hologram, a collector lens, and a CCD. Again, the agreement between the theoretical and the experimental results was very good. Using the theoretical models, we showed that the slitless spectrometer is a compact implementation of the conventional spectrometer when the slit is implemented by the Bragg selectivity of the volume hologram and that the function of the collimating lens is included in the SBVH. Therefore the proposed method enables us to make compact and low-cost spectrometers suitable for portable applications. Since the hologram is placed at the input of the spectrometer, light can easily couple into the device.

We also showed that the slitless architecture has more design flexibility, as the dependency of the performance on the design parameters is different from that of the conventional spectrometer. In particular, we showed that the wavelength range of operation depends on the recording parameters of the SBVH (basically, the divergence angle of the recording spherical beam) in the slitless spectrometer in contrast to that dependency on the thickness of the holographic material in the conventional spectrometer. We also showed that the resolution of the slitless spectrometer is a function of hologram thickness and that it is possible to design an optimal spectrometer by simply recording an optimal volume hologram, which does not add to the hardware complexity of the spectrometer.

This research was supported by the National Institute on Alcohol Abuse and Alcoholism through the Integrated Alcohol Sensing and Data Analysis program under contract N01-AA-23013 and by the David and Lucile Packard Foundation. The authors thank Babak Momeni and Arash Karbaschi for their helpful discussions.

References

1. R. G. Bingham, "Grating spectrometers and spectrographs reexamined," Q. J. R. Astron. Soc. **20,** 395–421 (1979).
2. S. Singh, "Diffraction gratings: aberrations and applications," Opt. Laser Technol. **31,** 195–218 (1999).
3. C. Hsieh, O. Momtahan, A. Karbaschi, A. Adibi, M. E. Sullivan, and D. J. Brady, "A compact Fourier transform volume holographic spectrometer for diffuse source spectroscopy," Opt. Lett. **30,** 836–838 (2005).
4. W. Cassarly, "Nonimaging optics: concentration and illumination," in *OSA Handbook of Optics,* 2nd ed. (McGraw-Hill, 2001), Vol. 3, Chap. 2.
5. D. J. Brady, "Multiplex sensors and the constant radiance theorem," Opt. Lett. **27,** 16–18 (2002).
6. A. Karbaschi, C. Hsieh, O. Momtahan, A. Adibi, M. E. Sullivan, and D. J. Brady, "Qualitative demonstration of spectral diversity filtering using spherical beam volume holograms," Opt. Express **12,** 3018–3024 (2004).
7. O. Momtahan, C. Hsieh, A. Karbaschi, A. Adibi, M. E. Sullivan, and D. J. Brady, "Spherical beam volume holograms for spectroscopic applications: modeling and implementation," Appl. Opt. **43,** 6557–6567 (2004).
8. C. Hsieh, O. Momtahan, A. Karbaschi, A. Adibi, M. E. Sullivan, and D. J. Brady, "Role of recording geometry in the performance of spectral diversity filters using spherical beam volume holograms," Opt. Lett. **30,** 186–188 (2005).
9. J. W. Goodman, *Introduction to Fourier Optics,* 2nd ed. (McGraw-Hill, 1996).
10. G. Barbastathis and D. Psaltis, "Volume holographic multiplexing methods," in *Holographic Data Storage*, H. J. Coufal, D. Psaltis, and G. T. Sincerbox, eds. (Springer, 2000), pp. 21–59.
11. H. Kogelnik, "Coupled wave theory for thick hologram gratings," Bell Syst. Tech. J. **48,** 2909–2947 (1969).
12. T. K. Gaylord and M. G. Moharam, "Analysis and applications of optical diffraction by gratings," Proc. IEEE **73,** 894–937 (1985).
13. R. T. Ingwall and D. Waldman, "Photopolymer systems," in *Holographic Data Storage,* H. J. Coufal, D. Psaltis, and G. T. Sincerbox, eds. (Springer, 2000), pp. 171–197. Also see www.aprilisinc.com.